This is an Accepted Manuscript of an article published by IEEE in IEEE Transactions on Vehicular Technology in January 2018, available online: DOI:10.1109/TVT.2017.2744604.

A Mathematical Model of Multi-Speed Transmissions in Electric Vehicles in the Presence of Gear-Shifting

Yuhanes Dedy Setiawan, Mehdi Roozegar, Ting Zou, and Jorge Angeles, *Fellow, IEEE*[*†]

***Abstract*—Some studies indicate the potential of multi-speed transmissions (MSTs) in improving performance of electric vehicles (EVs), which has led to many developments of MSTs in this context. However, comprehensive dynamics analyses have not been reported yet. For this reason, a mathematical model for MSTs in EVs is being developed, as reported in this paper. This model will be beneficial to support the design and control of EV-oriented MSTs. The transient dynamic response of the transmission is of interest in this study. Therefore, backlash, flexibility and dissipation of the gear mesh and connecting parts between two planetary gear sets are studied, while taking all these items into account. The system topology variations induced upon gear-shifting are given due attention. Simulation results are validated with experiments. The results show that the model can provide a realistic dynamic response of the transmission.**

***Index Terms*—Mathematical model, multi-speed transmissions, dynamic response, electric vehicles, gear-shifting.**

I. Introduction

ELECTRIC vehicles (EVs) appear as the best alternatives to internal-combustion-engine vehicles (ICEVs) [1, 2]. R&D of EVs began since they were first commercialized by the end of the 19th century [3]. The main purpose of the R&D work in this context is to replace fossil-fuel engines with electric motors (EMs), in order to reduce greenhouse-gas emission and improve efficiency [4]. Developments have not only occurred in the vehicle system [5–8], but also in energy consumption [9, 10]. The main focus in this study is electric trucks, especially in the medium- and heavy-duty categories (EMHTs).

Trucks in general have been utilized widely for short- and long-haul delivery. Consequently, electrification and hybridization have been attractive options due to the high energy consumption and gas emission in trucks. There are more than eight companies all over the world manufacturing EMHTs. In the same way, R&D of EMHTs has been conducted to improve their performance, particularly the application of multi-speed transmissions (MSTs). Carrying heavy loads, EMHTs need to be equipped with large EMs, which may not be feasible economically. Application of MSTs can solve the situation by downsizing the motors. Several companies, such as EMOSS, Electric Vehicle International and Balqon, have produced EMHTs with a transmission. Other companies, such as Hytruck, Motiv Power Systems, and Smith Electric Vehicles, have dispensed with mechanical transmissions in their EMHTs on the basis that EMs have a wide range of operation, as required by trucks, thereby obviating transmissions. This is, therefore, still a controversial issue because it is unclear whether a transmission in EMHTs, or EVs in general, is necessary at all [11].

Many works have confirmed the contribution of a transmission to the improvement of EV performance [12–17]. From experiments conducted to verify transmission performance in EVs, Roberts [14] found that MSTs could keep the EMs operating at the most efficient region with an efficiency higher than 90%. Besides, Roberts' tests demonstrated that the transmission increased the efficiency by 15% under the New European Driving Cycle (NEDC). Other researchers [15–18] reported the significant contribution of transmissions to EV performance under simulation.

Although many research efforts in MSTs for EVs have been reported, thorough dynamics analyses that support the design and control of MSTs for EVs are still to appear in the literature. These analyses represent an important stage in transmission design and development to understand the dynamic response of the transmission and to determine, by simulation, whether the transmission will work effectively within the intended operation range and under given conditions. Dynamics analyses to achieve optimal MST design have been conducted extensively since the inception of ICEVs. These analyses could be a reference for the analyses of MST in EVs, but not entirely, because MSTs for ICEVs and those for EVs are inherently different, mainly because of the differences in the energy source. This leads to several different features in MSTs for EVs, such as regenerative braking, no clutch/torque converter between motor and MSTs, and no reverse gear. For this reason, the dynamics analysis of MSTs in EVs under gear-shifting needs to be investigated on its own merit. The first step of this analysis is to develop the system mathematical model. This model can provide the dynamic response of the system, which is important to support optimal transmission design, gear-shifting analysis and vibration analysis [19]. In addition, these are intended to be beneficial for researchers and/or engineers for the development and validation of shifting schedules and control systems. The major research challenge in this context is that the system topology changes during gear-shifting; models with time-varying topology are thus needed. The objective of this research is to develop a mathematical model for the dynamic response of MSTs in EVs under gear-

[*]Y. D. Setiawan, M. Roozegar, T. Zou and J. Angeles are with the Centre for Intelligent Machines (CIM) and Department of Mechanical Engineering, McGill Unviversity, Montréal, QC, H3A 0C3 Canada e-mails: dedy@cim.mcgill.ca, roozegar@cim.mcgill.ca, ting@cim.mcgill.ca, angeles@cim.mcgill.ca

[†]Manuscript received XXX; revised XXX.

shifting.

Transmission models consist of inertial elements, gear meshing, and elements that are capable of either storing or dissipating energy. Transverse-torsional models have been developed for planetary gear sets (PGSs) [20–25] and are proven effective for representing the PGS dynamic response. However, transversal motion may be dispensable for vibration analysis when the supporting-bearing stiffness is tenfold larger than mesh stiffness [26], meaning that gears are not allowed to float. Another way to model planetary gear sets is by means of Finite Element (FE) models [27–30]. However, for the purpose of this study, FE models are not needed, as lumped-parameter models have been proven effective for representing PGSs [24]. Therefore, our study is based on torsional lumped-parameter models.

Kahraman [31] formulated a set of torsional-dynamics models of compound gear sets using a Lagrangian formulation to predict free-vibration characteristics under different transmission topologies. To account for backlash in the gear system, Al-shyyab and Kahraman [32] developed further Kahraman's model by including a periodic variation of gear backlash. Torsional springs were then added to represent the component coupling between two adjacent gear sets [33, 34]. Furthermore, Inalpolat and Kahraman [35] applied Kahraman's model [31] to automatic transmissions where a generalized model for its multi-stage planetary gear trains is developed. However, backlash is not included in this study, while the mathematical models were not validated experimentally.

A mathematical model is developed in this paper for MSTs in EVs, based on Inalpolat and Kahraman's model, with the addition of dashpots and backlash to account for dissipation and backlash in the gear mesh. The model is developed for a specific MST, but the approach can be applied to other kinds of MSTs as well. A Simulink model is then built to validate the effectiveness of the model. The dynamic response during gear-shifting is predicted and analyzed. A testbed is built and developed to later confirm the simulation results.

II. Transmission System

Most automatic transmissions are composed of planetary gear sets; therefore, this type is chosen for this study. For quick reference, a simple PGS is illustrated in Fig. 1(a). In general, a simple PGS has four components: a sun gear; a planet gear; a ring gear; and "the carrier". The MST considered in this work comprises an input motor, a load, and two identical planetary gear trains connected by the carrier [18]; the train connected to the motor is referred to as *underdrive*, whereas that connected to the load as *overdrive*, with the whole MST depicted in Fig. 1(b). Furthermore, two kinds of clutches are utilized, a ring clutch and a carrier clutch. The former is used to stop the ring gears, the latter to connect the carrier to the sun shafts.

Multiple PGSs can be installed in both the underdrive and the overdrive gear trains. The number of speed ratios of a transmission depends on the number of PGSs installed in the transmission. A MST consisting of two in-parallel-connected PGSs in both underdrive and overdrive is considered in this study. Each PGS carries three planet gears. Functional and graph representations of the MST are shown in Figs. 2 and 3, respectively. The first and second underdrive sun gears are connected via a common sun gear shaft; those in the overdrive are connected likewise. A long common carrier connects the four PGS from underdrive to overdrive. A graph representation of the transmission, shown in Fig. 3, is used to give a better understanding of the system topology. The mechanism consists of 11 inertia elements (IE), four revolute pairs, eight gear pairs (meshings), two carrier clutches, and four ring clutches. The IEs are numbered from 1 to 11. The IEs and the kinematic joints are represented as nodes and edges, respectively, the gear pairs represented by dashed lines and the revolute pairs by solid edges. These figures show the system condition when all clutches are open. When a clutch is closed, the system topology and its mathematical model change accordingly. The topology change can be seen from the representations for the first operation mode, as depicted in Fig. 4.

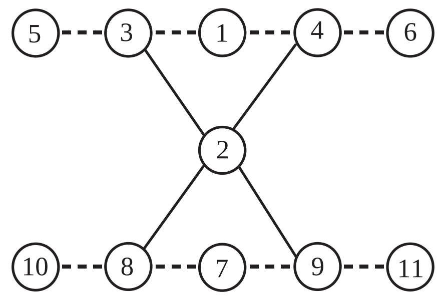

Fig. 3: Graph representation of the transmission

III. Mathematical Model

First, generic models will be formulated for n gear sets. With reference to Kahraman's work [31, 35], an initial model was formulated under the assumptions below:

1) Sun gears, planet gears, and ring gears are modelled as rigid disks with teeth in their periphery, which mesh by means of linearly viscoelastic elements;
2) All clutches are modelled as rigid, passive elements, capable of dissipating energy only at the inception of closing or opening;
3) The relative displacements of the planet gears in a planetary gear set with respect to their common sun gear are identical;
4) Only one tooth pair is assumed to be in contact;
5) Radial deflection of bearing supports in the sun gear, ring gear, planet gear, and the carrier are negligible;
6) Mesh stiffness is constant.

The generalized coordinates are the angular displacements of the IEs (sun gears, planet gears, carrier, and ring gears) in the underdrive and overdrive gear trains. Gear mesh contact is modelled with (i) springs, to account for the potential energy stored in the deformed gear teeth and (ii) dashpots, to account for dissipation, as depicted in Fig. 5. Moreover, torsional springs are used to represent the flexibilities of sun shafts and carrier; the latter is located between the planet gears. Unless otherwise specified, subscripts i and j stand for the gear train

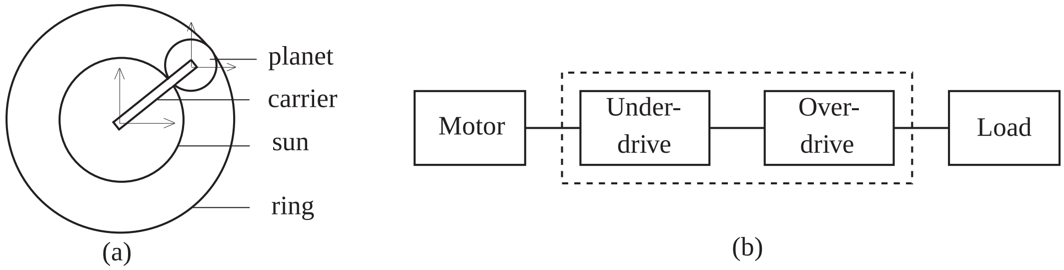

Fig. 1: (a) A simple PGS; (b) a diagram of the MST

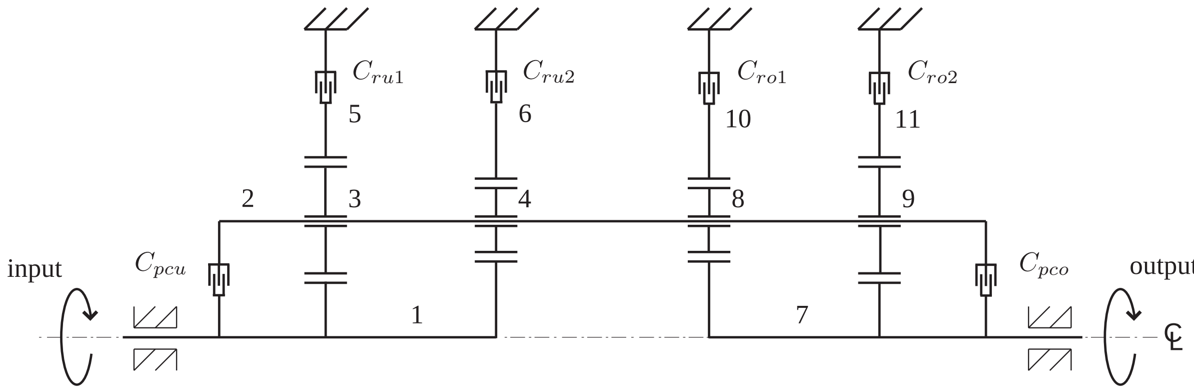

Fig. 2: Functional representation of the transmission

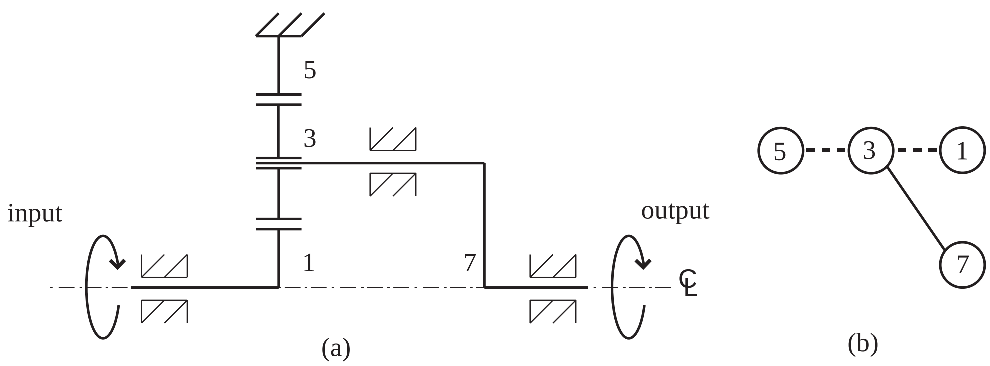

Fig. 4: The first operation mode: (a) functional and (b) graph representation

and the stage, respectively, with the former being either o for overdrive or u for underdrive, the latter either 1 or 2. The parameter definition is given in Table 1 in the Appendix. The equations of motion can be expressed in array form as:

$$\mathbf{M}\ddot{\mathbf{q}} + \mathbf{C}\dot{\mathbf{q}} + \mathbf{K}\mathbf{q} = \mathbf{f} \tag{1}$$

where $\mathbf{q}$ is the 16-dimensional vector of independent generalized coordinates, with the definitions below:

$$\mathbf{q} = \begin{bmatrix} \mathbf{q}_u \\ \mathbf{q}_o \end{bmatrix} \in \mathbb{R}^{16}, \quad \mathbf{q}_i = \begin{bmatrix} \mathbf{q}_{i1} \\ \mathbf{q}_{i2} \end{bmatrix} \in \mathbb{R}^8, \ i = u, o,$$

$$\mathbf{q}_{ij} = \begin{bmatrix} q_{sij} \\ q_{pij} \\ q_{cij} \\ q_{rij} \end{bmatrix} \in \mathbb{R}^4$$

Furthermore, $\mathbf{f}$ is the 16-dimensional vector of generalized forces, whereas $\mathbf{M}$, $\mathbf{C}$ and $\mathbf{K}$ are the 16×16 mass, damping and stiffness matrices, respectively. $\mathbf{M}$ is calculated as the Hessian matrix of the kinetic energy T with respect to $\dot{\mathbf{q}}$, $\mathbf{C}$ as the Hessian matrix of the dissipation function Δ with respect to $\dot{\mathbf{q}}$, and $\mathbf{K}$ as the Hessian matrix of the potential energy V with respect to $\mathbf{q}$.

The kinetic energy of the system is the sum of those in the two subsystems, underdrive and overdrive.

$$T = T_u + T_o \tag{2}$$

where

$$T_u = T_{u1} + T_{u2}$$

The first and second terms T_{u1} and T_{u2} describe the kinetic energies of the first and the second planetary gear sets in the underdrive gear train, which stem from translation of the planet gears and rotation of the sun gears, planet gears, carrier and

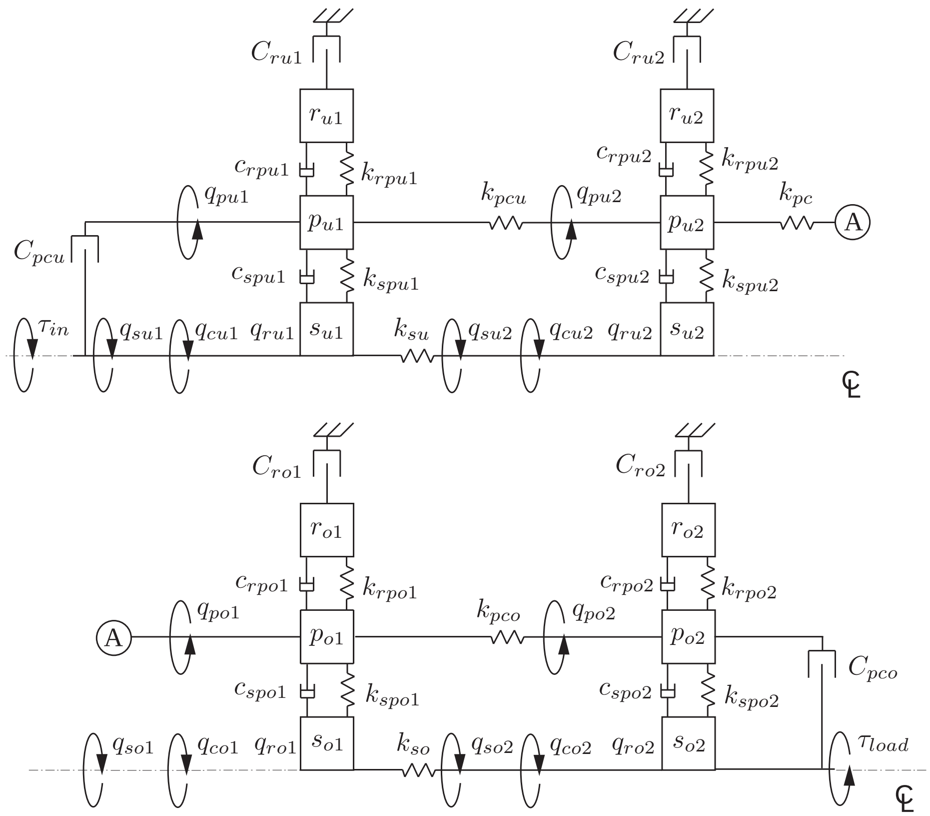

Fig. 5: The iconic model of the transmission

ring gears about the system centerline, as illustrated in Fig. 5. Since three planet gears are used in each gear set, the kinetic energies associated with the planet gears are multiplied by 3, as shown below

$$T_{u1} = \frac{1}{2} I_{su1} \dot{q}_{su1}^2 + 3 I_{pu1} \dot{q}_{pu1} \dot{q}_{cu1} + \frac{3}{2} I_{pu1} \dot{q}_{pu1}^2 + \frac{1}{2} I_{pcu1} \dot{q}_{cu1}^2 + \frac{1}{2} I_{ru1} \dot{q}_{ru1}^2$$

$$T_{u2} = \frac{1}{2} I_{su2} \dot{q}_{su2}^2 + 3 I_{pu2} \dot{q}_{pu2} \dot{q}_{cu2} + \frac{3}{2} I_{pu2} \dot{q}_{pu2}^2 + \frac{1}{2} I_{pcu2} \dot{q}_{cu2}^2 + \frac{1}{2} I_{ru2} \dot{q}_{ru2}^2$$

with the inertia of the planet carrier being

$$I_{pcij} = I_{cij} + n I_{pij} + n m_{pij} r_{cij}^2 \tag{3}$$

where n is the number of planet gears and m_{pij} the planet gear mass.

Likewise, the kinetic energy of the overdrive is

$$T_o = T_{o1} + T_{o2}$$

where T_{o1} and T_{o2} describe the kinetic energies of the first and the second planetary gear sets in the overdrive gear train, which stem from translation of the planet gears and rotation of the sun gears, planet gears, carrier and ring gears about the system centerline, as shown below.

$$T_{o1} = \frac{1}{2} I_{so1} \dot{q}_{so1}^2 + 3 I_{po1} \dot{q}_{po1} \dot{q}_{co1} + \frac{3}{2} I_{po1} \dot{q}_{po1}^2 + \frac{1}{2} I_{pco1} \dot{q}_{co1}^2 + \frac{1}{2} I_{ro1} \dot{q}_{ro1}^2$$

$$T_{o2} = \frac{1}{2} I_{so2} \dot{q}_{so2}^2 + 3 I_{po2} \dot{q}_{po2} \dot{q}_{co2} + \frac{3}{2} I_{po2} \dot{q}_{po2}^2 + \frac{1}{2} I_{pco2} \dot{q}_{co2}^2 + \frac{1}{2} I_{ro2} \dot{q}_{ro2}^2$$

Thus, the mass matrix is readily found as

$$\mathbf{M} = \begin{bmatrix} \mathbf{I}_u & \mathbf{O}_{8\times 8} \\ \mathbf{O}_{8\times 8} & \mathbf{I}_o \end{bmatrix} \tag{4}$$

where

$$\mathbf{I}_i = \begin{bmatrix} \mathbf{I}_{i1} & \mathbf{O}_{4\times 4} \\ \mathbf{O}_{4\times 4} & \mathbf{I}_{i2} \end{bmatrix}, \quad \mathbf{I}_{ij} = \begin{bmatrix} I_{sij} & 0 & 0 & 0 \\ 0 & 3I_{pij} & 3I_{pij} & 0 \\ 0 & 3I_{pij} & I_{pcij} & 0 \\ 0 & 0 & 0 & I_{rij} \end{bmatrix}$$

with $\mathbf{O}_{m\times n}$ denoting the the $m \times n$ zero matrix, and all non-zero entries of I_{ij} defined in Table 1 in the Appendix.

The system potential energy is the sum of all individual potential energies of elements that are capable of storing potential energy. The potential energy of the system is divided into two parts: potential energy in the underdrive gear train and that in its overdrive counterpart, namely,

$$V = V_u + V_o \tag{5}$$

The above terms come from two sources: contact between the gears and flexibility of the sun shafts and the connecting parts of the carrier. Since three planet gears are used in each gear set, the potential energies of the gear contact are multiplied by 3. Changes in the potential energy due to gravity are assumed to be negligible because the components only revolve around the system centerline, and all are assumed to be statically balanced. As well, the three planets are laid out symmetrically, at equal angles of 120°, the center of mass of the three planets thus remaining fixed. Relative gear mesh displacements δ are used; δ_s accounts for relative gear mesh displacements between sun gear and planet gear, whereas δ_r for that between planet gear and ring gear. Hence,

$$\begin{aligned}
V_u &= V_{u1} + V_{u2}\\
V_{u1} &= \frac{3}{2}k_{spu1}\delta_{su1}^2 + \frac{3}{2}k_{rpu1}\delta_{ru1}^2 + \frac{1}{2}k_{su}\left(q_{su1} - q_{su2}\right)^2\\
&\quad + \frac{1}{2}k_{pcu}\left(q_{cu1} - q_{cu2}\right)^2\\
V_{u2} &= \frac{3}{2}k_{spu2}\delta_{su2}^2 + \frac{3}{2}k_{rpu2}\delta_{ru2}^2 + \frac{1}{2}k_{pc}\left(q_{cu2} - q_{co1}\right)^2
\end{aligned}$$

$$\begin{aligned}
V_o &= V_{o1} + V_{o2}\\
V_{o1} &= \frac{3}{2}k_{spo1}\delta_{so1}^2 + \frac{3}{2}k_{rpo1}\delta_{ro1}^2 + \frac{1}{2}k_{so}\left(q_{so1} - q_{so2}\right)^2\\
&\quad + \frac{1}{2}k_{pco}\left(q_{co1} - q_{co2}\right)^2\\
V_{o2} &= \frac{3}{2}k_{spo2}\delta_{so2}^2 + \frac{3}{2}k_{rpo2}\delta_{ro2}^2
\end{aligned}$$

Each δ for the whole system is stored in array $\boldsymbol{\delta}$ as

$$\boldsymbol{\delta} = \mathbf{R}\mathbf{q} \tag{6}$$

where

$$\boldsymbol{\delta} = \begin{bmatrix}\delta_{su1} & \delta_{ru1} & \delta_{su2} & \delta_{ru2} & \delta_{so1} & \delta_{ro1} & \delta_{so2} & \delta_{ro2}\end{bmatrix}^T$$

$$\mathbf{R} = \begin{bmatrix}\mathbf{R}_u & \mathbf{O}_{4\times8}\\ \mathbf{O}_{4\times8} & \mathbf{R}_o\end{bmatrix} \in \mathbb{R}^{8\times16},$$

$$\mathbf{R}_i = \begin{bmatrix}\mathbf{R}_{i1} & \mathbf{O}_{2\times4}\\ \mathbf{O}_{2\times4} & \mathbf{R}_{i2}\end{bmatrix} \in \mathbb{R}^{4\times8},$$

$$\mathbf{R}_{ij} = \begin{bmatrix} r_{si1} & r_{pi1} & -(r_{si1} + r_{pi1}) & 0\\ 0 & -r_{pi1} & r_{pi1} - r_{ri1} & r_{ri1}\end{bmatrix}$$

with all parameters defined in Table 1 in the Appendix.

In order to clearly express the stiffness matrix, the total potential energy in Eq. (5) is decomposed into two parts, V_c and V_f, denoting the potential energy due to the gear contact and that due to the flexibility of the carrier and the sun shafts, respectively:

$$\begin{aligned}
V_c = &\frac{3}{2}k_{spu1}\delta_{su1}^2 + \frac{3}{2}k_{rpu1}\delta_{ru1}^2 + \frac{3}{2}k_{spu2}\delta_{su2}^2\\
&+ \frac{3}{2}k_{rpu2}\delta_{ru2}^2 + \frac{3}{2}k_{spo1}\delta_{so1}^2 + \frac{3}{2}k_{rpo1}\delta_{ro1}^2\\
&+ \frac{3}{2}k_{spo2}\delta_{so2}^2 + \frac{3}{2}k_{rpo2}\delta_{ro2}^2
\end{aligned}$$

$$\begin{aligned}
V_f = &\frac{1}{2}k_{su}\left(q_{su1} - q_{su2}\right)^2 + \frac{1}{2}k_{pcu}\left(q_{cu1} - q_{cu2}\right)^2\\
&+ \frac{1}{2}k_{pc}\left(q_{cu2} - q_{co1}\right)^2 + \frac{1}{2}k_{so}\left(q_{so1} - q_{so2}\right)^2\\
&+ \frac{1}{2}k_{pco}\left(q_{co1} - q_{co2}\right)^2
\end{aligned}$$

The total stiffness matrix, which comprises the stiffness matrix due to gear contact, $\mathbf{K}_c$, and that due to the flexibility of the carrier and the sun shafts, $\mathbf{K}_f$, is thus readily calculated, namely,

$$\mathbf{K} = \mathbf{K}_c + \mathbf{K}_f = \frac{\partial^2 V_c}{\partial \mathbf{q}^2} + \frac{\partial^2 V_f}{\partial \mathbf{q}^2} \quad \in \mathbb{R}^{16\times16} \tag{7}$$

and

$$\mathbf{K}_c = \begin{bmatrix}\mathbf{K}_{cu} & \mathbf{O}_{8\times8}\\ \mathbf{O}_{8\times8} & \mathbf{K}_{co}\end{bmatrix}, \text{with} \quad \mathbf{K}_{ci} = \begin{bmatrix}\mathbf{K}_{ci1} & \mathbf{O}_{4\times4}\\ \mathbf{O}_{4\times4} & \mathbf{K}_{ci2}\end{bmatrix}, \quad i = u, o$$

Moreover,

$$\mathbf{K}_{cij} = \begin{bmatrix} k_1 & k_2 & k_3 & 0\\ k_2 & k_4 & k_5 & k_6\\ k_3 & k_5 & k_7 & k_8\\ 0 & k_6 & k_8 & k_9\end{bmatrix} \tag{8}$$

where

$$\begin{aligned}
&k_1 = 3k_{spij}r_{sij}^2, \quad k_2 = 3k_{spij}r_{sij}r_{pij},\\
&k_3 = -3k_{spij}r_{sij}(r_{pij} + r_{sij}), \quad k_4 = 3(k_{spij} + k_{rpij})r_{pij}^2,\\
&k_5 = -3r_{pij}k_{spij}(r_{pij} + r_{sij}) - 3r_{pij}k_{rpij}(r_{pij} - r_{rij}),\\
&k_6 = -3k_{rpij}r_{pij}r_{rij},\\
&k_7 = 3k_{spij}(r_{pij} + r_{sij})^2 + 3k_{rpij}(r_{pij} - r_{rij})^2,\\
&k_8 = 3k_{rpij}r_{rij}(r_{pij} - r_{rij}), \quad k_9 = 3k_{rpij}r_{rij}^2
\end{aligned}$$

and all parameters defined in Table 1 in the Appendix.

Further, $\mathbf{K}_f$ is readily obtained as

$$\mathbf{K}_f = \begin{bmatrix}\mathbf{K}_{fu} & \mathbf{K}_{f1}\\ \mathbf{K}_{f1}^T & \mathbf{K}_{fo}\end{bmatrix} \tag{9}$$

where

$$\mathbf{K}_{fu} = \begin{bmatrix}\mathbf{K}_{fu1} & -\mathbf{K}_{fu1}\\ -\mathbf{K}_{fu1} & \mathbf{K}_{fu2}\end{bmatrix}, \quad \mathbf{K}_{fo} = \begin{bmatrix}\mathbf{K}_{fo2} & -\mathbf{K}_{fo1}\\ -\mathbf{K}_{fo1} & \mathbf{K}_{fo1}\end{bmatrix},$$

$$\mathbf{K}_{f1} = \begin{bmatrix}\mathbf{O}_{4\times4} & \mathbf{K}_{fu1} - \mathbf{K}_{fu2}\\ \mathbf{O}_{4\times4} & \mathbf{O}_{4\times4}\end{bmatrix}$$

and

$$\mathbf{K}_{fi1} = \begin{bmatrix} k_{si} & 0 & 0 & 0 \\ 0 & 0 & 0 & 0 \\ 0 & 0 & k_{pci} & 0 \\ 0 & 0 & 0 & 0 \end{bmatrix},$$

$$\mathbf{K}_{fi2} = \begin{bmatrix} k_{si} & 0 & 0 & 0 \\ 0 & 0 & 0 & 0 \\ 0 & 0 & k_{pci} + k_{pc} & 0 \\ 0 & 0 & 0 & 0 \end{bmatrix}, \quad i = u, o$$

with all parameters in the foregoing arrays defined in Table 1 in the Appendix.

A motor is coupled to the underdrive sun shaft of the first gear set to supply power, while a load is coupled to the overdrive sun shaft of the second gear set. Moreover, each ring gear has a resisting torque to hold the ring gear. Thus, the generalized force **f** is expressed in (10), shown at the bottom of the page.

Contact between gears dissipates power. The power dissipated due to contact is represented by dashpots at each pair of meshing gears. The power dissipated in the underdrive and overdrive gear trains yields the total power dissipated:

$$\Delta = \Delta_u + \Delta_o, \quad \Delta_u = \Delta_{u1} + \Delta_{u2}, \quad \Delta_o = \Delta_{o1} + \Delta_{o2}$$

where

$$\Delta_{u1} = \frac{3}{2} c_{spu1} \dot{\delta}_{su1}^2 + \frac{3}{2} c_{rpu1} \dot{\delta}_{ru1}^2$$
$$\Delta_{u2} = \frac{3}{2} c_{spu2} \dot{\delta}_{su2}^2 + \frac{3}{2} c_{rpu2} \dot{\delta}_{ru2}^2$$
$$\Delta_{o1} = \frac{3}{2} c_{spo1} \dot{\delta}_{so1}^2 + \frac{3}{2} c_{rpo1} \dot{\delta}_{ro1}^2$$
$$\Delta_{o2} = \frac{3}{2} c_{spo2} \dot{\delta}_{so2}^2 + \frac{3}{2} c_{rpo2} \dot{\delta}_{ro2}^2$$

The damping matrix is readily identified as

$$\mathbf{C} = \begin{bmatrix} \mathbf{C}_u & \mathbf{O}_{8\times4} \\ \mathbf{O}_{8\times4} & \mathbf{C}_o \end{bmatrix},$$

with

$$\mathbf{C}_i = \begin{bmatrix} \mathbf{C}_{i1} & \mathbf{O}_{4\times2} \\ \mathbf{O}_{4\times2} & \mathbf{C}_{i2} \end{bmatrix}, \quad i = u, o \tag{11}$$

Moreover,

$$\mathbf{C}_{cij} = \begin{bmatrix} c_1 & c_2 & c_3 & 0 \\ c_2 & c_4 & c_5 & c_6 \\ c_3 & c_5 & c_7 & c_8 \\ 0 & c_6 & c_8 & c_9 \end{bmatrix} \tag{12}$$

where

$$c_1 = 3c_{spij} r_{sij}^2, \quad c_2 = 3c_{spij} r_{sij} r_{pij},$$
$$c_3 = -3c_{spij} r_{sij}(r_{pij} + r_{sij}), \quad c_4 = 3(c_{spij} + c_{rpij}) r_{pij}^2,$$
$$c_5 = -3r_{pij} c_{spij}(r_{pij} + r_{sij}) - 3r_{pij} c_{rpij}(r_{pij} - r_{rij}),$$
$$c_6 = -3c_{rpij} r_{pij} r_{rij},$$
$$c_7 = 3c_{spij}(r_{pij} + r_{sij})^2 + 3c_{rpij}(r_{pij} - r_{rij})^2,$$
$$c_8 = 3c_{rpij} r_{rij}(r_{pij} - r_{rij}), \quad c_9 = 3c_{rpij} r_{rij}^2$$

The entries of the damping matrix **C** exhibit the same pattern as those of $\mathbf{K}_c$; therefore, **C** is symmetric and positive-definite as well.

A. Backlash Modelling

Backlash in the gear pair can be described with a simple gear pair, as shown in Fig. 6. The pinion in Fig. 6(a) has an input torque T_p and angular displacement q_p, whereas the gear has angular displacement q_g and an output torque T_g. The backlash in the gear tooth is illustrated in Fig. 6(b), where the deadband is represented by b. Figure 6(c) shows the characteristics of the backlash. The δ axis represents the gear mesh displacement, $\delta = q_g\ r_g - q_p\ r_p$, whereas the $f(\delta)$ axis the backlash model. The slope in Fig. 6c is the gear ratio r, which is lower than 1.0 for a simple gear pair, in general, as the purpose of a gear train is, generally, to operate as a speed reducer.

The backlash model is best described by a *normalized backlash* function bck(x), with a dead zone at $-1 \le x \le +1$, of unit slope, namely,

$$\mathrm{bck}(x) = -\rho(-x-1) + \rho(x-1) \tag{13}$$

where $\rho(\delta)$ represents the unit-ramp function [36].

Therefore, the backlash model of Fig. 6c can now be represented as

$$f(\delta) = r\ \mathrm{bck}(\delta; b) = r[-\rho(-\delta - b) + \rho(\delta - b)] \tag{14}$$

B. Friction Modelling

Friction coming from bearings and the gearhead must be taken into consideration. All friction sources are lumped and represented by a combination of Coulomb and viscous friction models. The characteristics of Coulomb friction, illustrated in Fig. 7, is modelled by a *saturation function* [37]. The Coulomb friction T_c equals the applied torque T_{app} when the latter is smaller than the static friction T_s. When T_{app} is equal to or larger than T_s, T_c equals T_s. The Coulomb friction is thus modelled as:

$$T_c = T_s\ \mathrm{sat}\left(\frac{T_{app}}{T_s}\right) \tag{15}$$

$$\mathbf{f} = \begin{bmatrix} \tau_{in} & 0 & 0 & \tau_1 & 0 & 0 & 0 & \tau_2 & 0 & 0 & 0 & \tau_3 & -\tau_{lo} & 0 & 0 & \tau_4 \end{bmatrix}^T \tag{10}$$

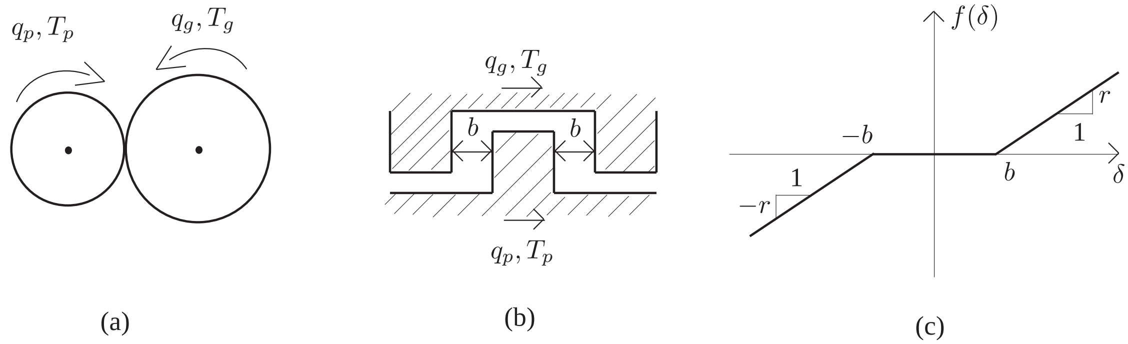

Fig. 6: (a) a simple gear pair, (b) backlash in the gear teeth, (c) backlash model

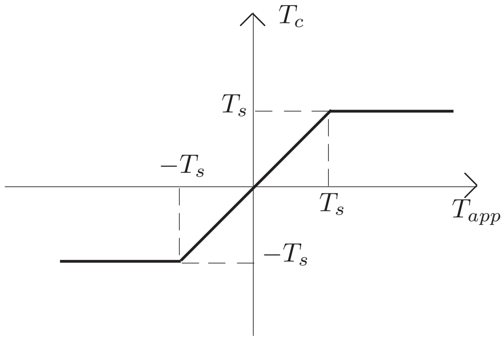

Fig. 7: Friction characteristics

where T_c is the Coulomb friction, T_{app} the applied torque, and T_s the static friction.

Furthermore, viscous friction T_v is proportional to the angular velocity, namely,

$$T_v = k_v \; \dot{q} \tag{16}$$

where k_v is the viscosity coefficient.

C. Topology Changes in the Model

The mathematical model in Eq. (1) undergoes topological changes, i.e., changes in dimension of vector $\mathbf{q}$ and, consequently, in the dimensions of the matrices occurring in the model, as the topology of the mechanical system, described by its graph in Figs. 3 and 4, changes upon gear-shifting [38]. To describe how topology changes affect these matrices and vectors, representations of the 16-dimensional vectors $\mathbf{q}$, $\dot{\mathbf{q}}$, $\ddot{\mathbf{q}}$, and $\mathbf{f}_f$, and the 16 × 16 matrices $\mathbf{M}$, $\mathbf{C}$, and $\mathbf{K}$ are shown in Fig. 8. The matrix entries that are eliminated when the ring clutch is closed are highlighted by the rectangles, and the notation of the four ring clutches (ru_1, ru_2, ro_1 and ro_2). For example, the first underdrive ring gear needs to be fixed to obtain the first operation mode of the transmission. Therefore, the generalized coordinate of the ring gear and its matrix entries are eliminated. The same is true for the overdrive ring gear. For the carrier-clutch, the corresponding sun gear and carrier columns will merge when the clutch is closed.

D. Modal Analysis

Natural frequencies and natural modes are important information to avoid powertrain resonance [20, 21]. For this reason, they are predicted for the system in Fig. 9 during the first speed ratio; an undamped system is first considered. The system is assumed to be amenable to a lumped-parameter model; therefore, the number of natural frequencies equals the degree of freedom (dof) of the system. In addition, in the interest of predicting natural frequencies, the unloaded planetary gear set acts merely as a load and, therefore, its dof is not taken into account. Thus, the system has four dof but when one of the ring gears is fixed, the dof reduces to three. The natural frequencies of the system were computed as 61.55, 213.864, and 1022.118 kHz. The normalized natural modes of the system are given below, the ith column corresponding to the ith natural frequency, for $i = 1, 2, 3$.

$$\mathbf{F}_{3dof} = \begin{array}{c} \begin{bmatrix} -0.0043 & -0.0132 & 1 \\ 1 & 1 & 0.002 \\ 0.0067 & -0.9491 & -0.0005 \end{bmatrix} \\ \begin{array}{ccc} \underbrace{\qquad\qquad}_{\text{first}} & \underbrace{\qquad\qquad}_{\text{second}} & \underbrace{\qquad\qquad}_{\text{third}} \end{array} \end{array}$$

IV. Simulation Results

A simulation of the underdrive gear train of the transmission illustrated in Fig. 9 was conducted to validate the model. In order to show the influence of backlash in the model, a sinusoidal input torque, depicted in Fig. 10, was applied. The input torque τ_{in} was transmitted to the first sun gear and the output torque was delivered through the carrier in the second set. No load is considered at this point. The gear ratios of the first and the second gear sets are 2.67:1 and 4:1, respectively. The simulated time span is 25 s. The first ring clutch, C_{ru1}, was closed for the first 12.5 s. After that, the clutch was released and the second ring clutch, C_{ru2}, was closed for another 12.5 s. The parameter values for the simulation are listed in Table II in the Appendix.

Simulation results are plotted in Figs. 11 and 12, describing the component angular velocities in the first PGS and those in the second PGS, respectively. The results show that the system moved at the desired speed ratios. The maximum input speed indicated by a is 267 rpm, whereas maximum output speed indicated by a' is 100 rpm; thereby proving the

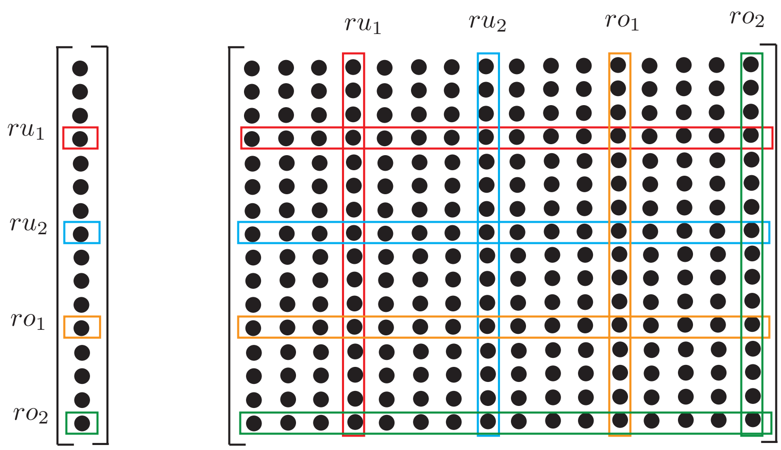

Fig. 8: Representation of vector $\mathbf{q}$ of generalized coordinates and its associated matrices ($\mathbf{M}$, $\mathbf{C}$ or $\mathbf{K}$)

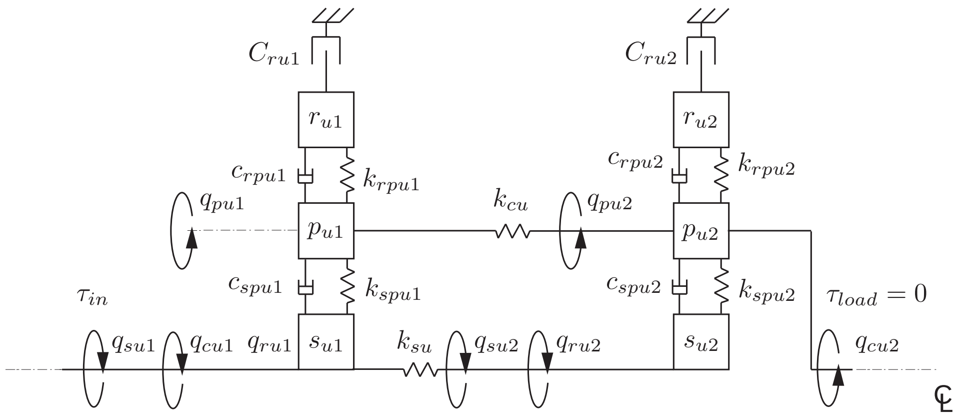

Fig. 9: The underdrive gear train of the transmission

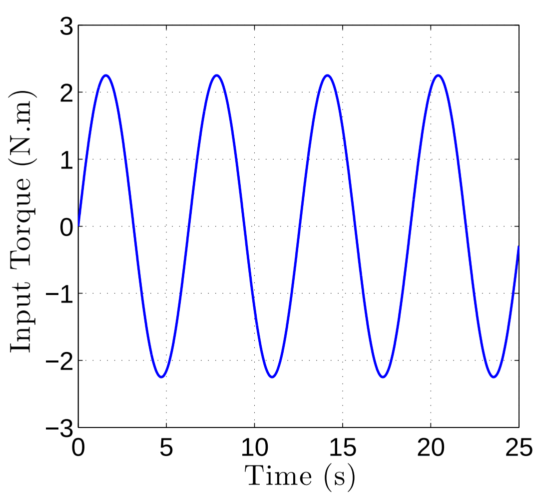

Fig. 10: Input torque

system rotated at a 2.67:1 ratio for the first 12.5 s. It then switched to 4:1 for another 12.5 s, indicated by b, which shows the maximum input speed 267 rpm and by b' showing the maximum output speed of 67 rpm. The gear-shifting can be observed from Figs. 11 and 12, where the first ring gear was held stationary for the first 12.5 s, then released; it was the other way around for the second ring gear. The impact of gear-shifting can also be observed in both figures, where the angular velocities of the ring gears affected those of other components. Moreover, the system had to stop for around 0.2 s each time it reversed direction. This stems from backlash and friction because the applied torque was not sufficient for overcoming the static friction. These results were validated experimentally, as detailed in Section V.

V. Experimental Work

A testbed of the transmission, shown in Fig. 13, was built and developed for validation purposes. Two Glentek brushless servomotors, GMBM80550-45 are utilized as the input and the load. Each servomotor is equipped with an encoder that produces angular-velocity readouts. A Q8 data-acquisition board is used to receive and send signals to the testbed. A PC under Windows XP is employed. The control system is built in Simulink, with an input torque signal sent to the testbed.

The underdrive gear train of the system was operated with the same input torque and procedure in the simulation; no load was given by the load motor. The input and output speeds are then compared with the simulation results individually in Figs. 14 and 15, respectively. The error between simulation and experimental results is also given in each figure. The dashed lines represent the simulation results, the solid lines the

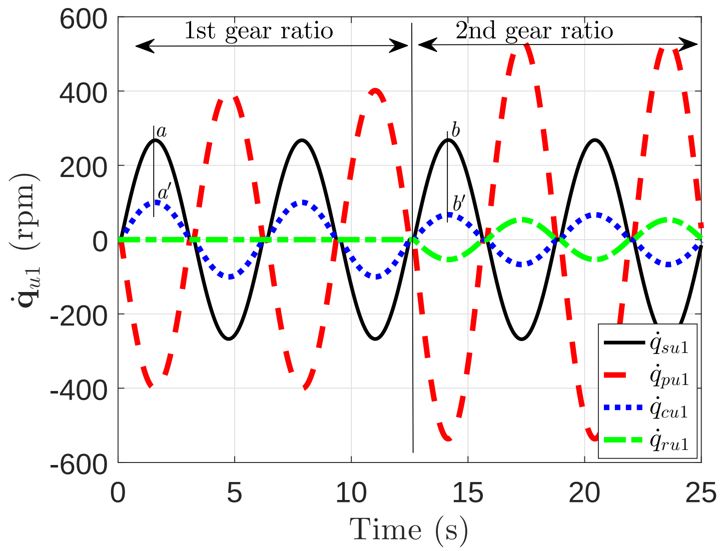

Fig. 11: Angular velocities of the first PGS

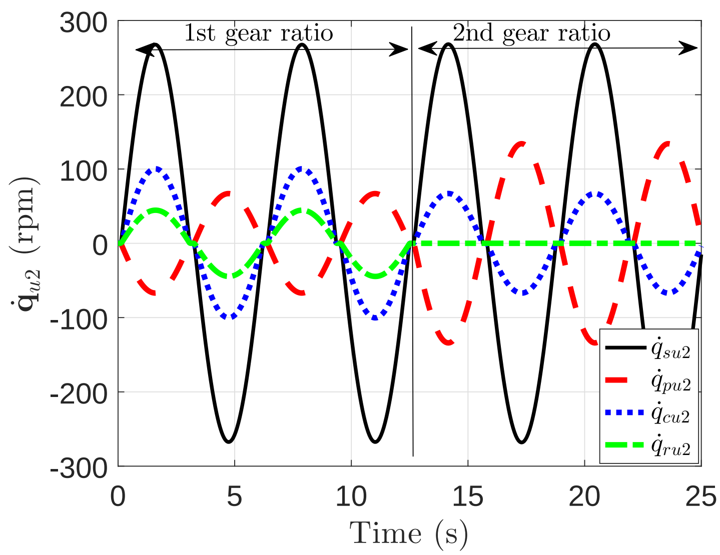

Fig. 12: Angular velocities of the second PGS

experimental results. It can be observed that the experimental results confirm the simulation results. The error is relatively small, as compared to the amplitude of the speed, of about 10 %.

VI. Conclusion

Dynamic analysis needs to be conducted for MSTs in EVs for purposes of design and control. A mathematical model for a MST comprising two gear trains and two PGSs for each train was developed, as reported in this paper. The model is topology-varying because MSTs have different topologies for each gear ratio. Furthermore, the transient dynamic response is of interest in this study, which requires that the model be as detailed as possible. To this end, dissipation and flexibility of the gear mesh were incorporated into the model, along with backlash. The approach is applicable to other MSTs. Simulation and experiments for the underdrive gear train of the transmission were conducted for validation. The results show the topology changes of the transmission and the pertinence of the model, which can provide a realistic dynamic response of the transmission under gear-shifting. The model is to support the design and control of MSTs in EVs.

Appendix

All parameters are defined in Table I. The parameter values used in simulation are listed in Table II.

Acknowledgment

The design and research work reported here was supported by a grant under Automotive Partnership Canada Project APCPJ418901-11. We also gratefully acknowledge the support of our industrial partners: Linamar, TM4 and Infolytica.

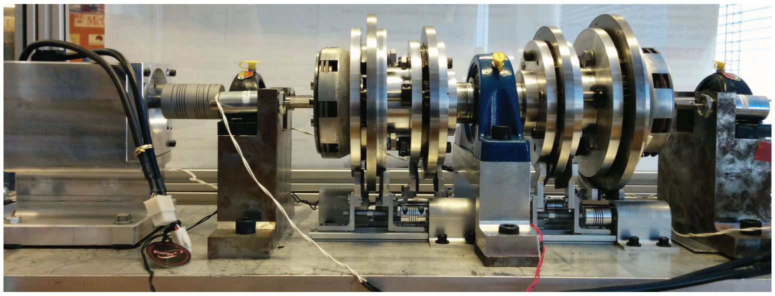

Fig. 13: The testbed

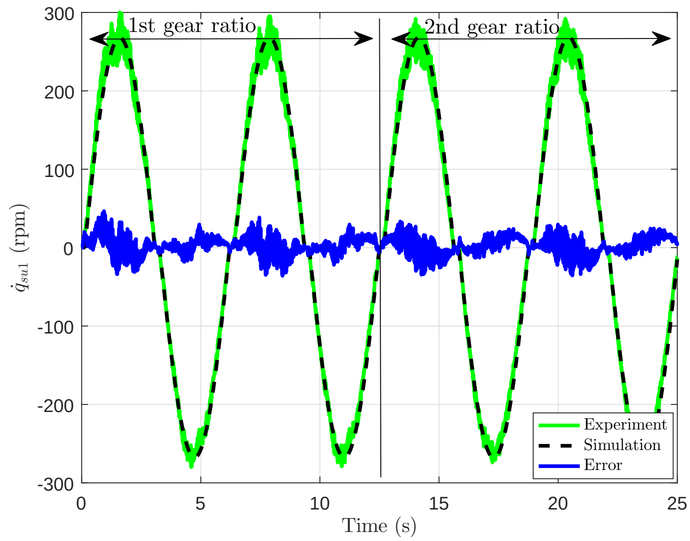

Fig. 14: Comparison of the input angular velocity, $\dot{q}_{su1}$, in simulation and experiment

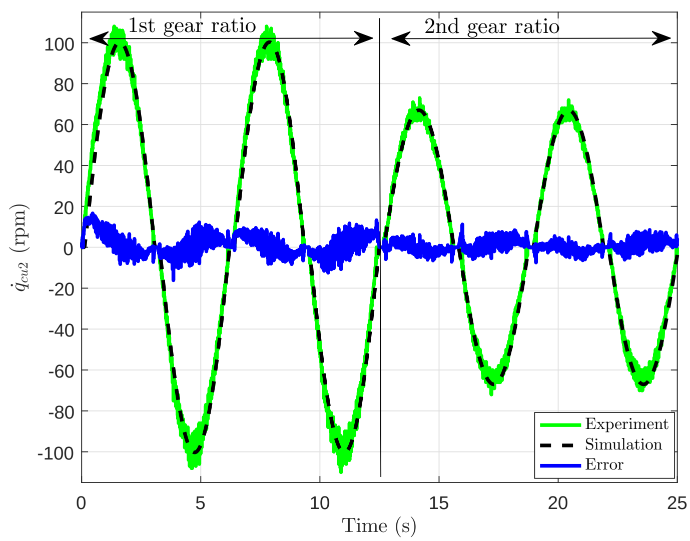

Fig. 15: Comparison of the output angular velocity, $\dot{q}_{cu2}$, in simulation and experiment

TABLE I: Parameter definition

Parameter	Definition
b	backlash deadband
c_{rpij}	damping coefficient of ring and planet gear mesh
c_{spij}	damping coefficient of sun and planet gear mesh
I_{cij}	polar mass moment of inertia of carrier
I_{pij}	polar mass moment of inertia of planet gear
I_{pcij}	polar mass moment of inertia of planet carrier
I_{rij}	polar mass moment of inertia of ring gear
I_{sij}	polar mass moment of inertia of sun gear
k_{pc}	spring coefficient of planet carrier between the underdrive and overdrive trains
k_{pco}	spring coefficient of planet carrier in the overdrive train
k_{pcu}	spring coefficient of planet carrier in the underdrive train
k_{rpij}	spring coefficient of ring and planet gear mesh
k_{so}	spring coefficient of the overdrive sun shaft
k_{spij}	spring coefficient of sun and planet gear mesh
k_{su}	spring coefficient of the underdrive sun shaft
r_{cij}	base circle radius of planet carrier
r_{pij}	base circle radius of planet gear
r_{rij}	base circle radius of ring gear
r_{sij}	base circle radius of sun gear

TABLE II: Simulation parameter values

Parameter	Value	Units		Parameter	Value	Units
c_{rp1}	820	Ns/m		I_{p1}	9.614×10^{-5}	kg m^2
c_{rp2}	820	Ns/m		I_{p2}	5.864×10^{-6}	kg m^2
c_{sp1}	820	Ns/m		I_{pc1}	0.0026	kg m^2
c_{sp2}	820	Ns/m		I_{pc1}	0.0061	kg m^2
r_{c1}	0.0508	m		I_{r1}	0.0132	kg m^2
r_{c2}	0.0508	m		I_{r2}	0.0082	kg m^2
r_{p1}	0.0239	m		I_{s1}	9.614×10^{-5}	kg m^2
r_{p2}	0.0119	m		I_{s2}	4.927×10^{-4}	kg m^2
r_{r1}	0.0716	m		k_{sp1}	2.56×10^{8}	N/m
r_{r2}	0.0597	m		k_{sp2}	2.56×10^{8}	N/m
r_{s1}	0.0239	m		k_{rp1}	3.87×10^{8}	N/m
r_{s2}	0.0358	m		k_{rp2}	3.87×10^{8}	N/m

References

[1] R. Schallenberg, "Prospects for the electric vehicle: a historical perspective," *IEEE Transactions on Education*, vol. 23, no. 3, pp. 137 – 143, 1980.

[2] B. Skugor and J. Deur, "A novel model of electric vehicle fleet aggregate battery for energy planning studies," *Energy*, vol. 92, no. 3, pp. 444 – 455, 2015.

[3] J. Larminie and J. Lowry, *Electric Vehicle Technology Explained*. Oxford Brookes U & Acenti Designs, West Sussex, England, 2003.

[4] I. Husain, *Electric and Hybrid Vehicles: Design Fundamentals, Second Edition*. Taylor and Francis, 2011.

[5] C. Mi, H. Lin, and Y. Zhang, "Iterative learning control of antilock braking of electric and hybrid vehicles," *IEEE Transactions on Vehicular Technology*, vol. 54, no. 2, pp. 486 – 494, 2005.

[6] B. Akin, S. Ozturk, H. Toliyat, and M. Rayner, "Dsp-based sensorless electric motor fault-diagnosis tools for electric and hybrid electric vehicle powertrain applications," *IEEE Transactions on Vehicular Technology*, vol. 58, no. 5, pp. 2150 – 2159, 2009.

[7] D. Kim, S. Hwang, , and H. Kim, "Vehicle stability enhancement of four-wheel-drive hybrid electric vehicle using rear motor control," *IEEE Transactions on Vehicular Technology*, vol. 57, no. 2, pp. 727 – 735, 2008.

[8] Y. Yang, J. Liu, T. Wang, K. Kuo, and P. Hsu, "An electric gearshift with ultracapacitors for the power train of an electric vehicle with a directly driven wheel motor," *IEEE Transactions on Vehicular Technology*, vol. 56, no. 5, pp. 2421 – 2431, 2007.

[9] H. Yoo, S. Sul, Y. Park, and J. Jeong, "System integration and power-flow management for a series hybrid electric vehicle using supercapacitors and batteries," *IEEE Transactions on Industry Application*, vol. 44, no. 1, pp. 108 – 114, 2008.

[10] S. Jung, H. Lee, C. Song, J. Han, W. Han, and G. Jang, "Optimal operation plan of the online electric vehicle system through establishment of a dc distribution system," *IEEE Transaction of Power Electronics*, vol. 28, no. 12, pp. 5878 – 5889, 2013.

[11] C. Chan and K. Chan, *Modern Electric Vehicle Technology*. Oxford University Press, 2001.

[12] L. Chen, F. Zhu, M. Zhang, Y. Huo, C. Yin, and H. Peng, "Design and analysis of an electrical variable transmission for a series-parallel hybrid electric vehicle," *IEEE Transactions on Vehicular Technology*, vol. 60, no. 5, pp. 2354 – 2363, 2011.

[13] A. Sorniotti, T. Holdstock, G. Pilone, F. Viotto, S. Bertolotto, M. Everitt, R. Barnes, B. Stubbs, and W. M., "Analysis and simulation of the gearshift methodology for a novel two-speed transmission system for electric powertrains with central motor," *Proceedings of the Institution of Mechanical Engineers, Part D: Journal of Automobile Engineering*, vol. 226, no. 7, pp. 915 – 929, 2012.

[14] S. Roberts, "Multispeed transmission for electric vehicles," *ATZ worldwide*, vol. 114, no. 4, pp. 8 – 11, 2012.

[15] A. Elmarakbi, A. Morris, Q. Ren, and M. Elkady, "Modelling and analyzing electric vehicles with geared transmission systems: enhancement of energy consumption and performance," *International Journal of Engineering Research and Technology*, vol. 2, no. 11, pp. 1215 – 1254, 2013.

[16] P. Walker, S. Rahman, B. Zhu, and N. Zhang, "Modelling, simulations, and optimisation of electric vehicles for analysis of transmission ratio selection," *Advances in Mechanical Engineering*, vol. 5, pp. 1 – 13, 2013.

[17] Q. Ren, D. Crolla, and A. Morris, "Effect of transmission design on electric vehicle performance," *Journal of Energy and Power Engineering*, vol. 4, no. 3, pp. 46 – 51, 2010.

[18] A. Morozov, T. Zou, M. Mousavi, Y. Setiawan, J. Angeles, and B. B., "Design and gear shift control of a modular swift-shift multi-speed transmission for evs," *European Battery, Hybrid and Fuel Cell Electric Vehicle Congress*, pp. 1 – 10, 2015.

[19] S. Bai, J. Maguire, and H. Peng, *Dynamic Analysis and Control System Design of Automatic Transmissions*. SAE International, 2013.

[20] D. R. Kiracofe and R. G. Parker, "Structured vibration modes of general compound planetary gear systems," *Journal of Vibration and Acoustics, Transactions of the ASME*, vol. 129, no. 1, pp. 1 – 16, 2007.

[21] J. Lin and R. Parker, "Analytical characterization of the unique properties of planetary gear free vibration," *Journal of Vibration and Acoustics, Transactions of the ASME*, vol. 121, no. 3, pp. 316 – 321, 1999.

[22] Y. Chen, J. Jin, and X. Wu, "Analysis of dynamical behavior of a planetary gear train," vol. 5314, pp. 46 – 53, 2008.

[23] B. Wang, Z. Lu, X. Chen, P. Wang, W. Luo, and H. Xu, "Modeling and analysis of the dynamic efficiency of manual transmission/reducer," *International Journal of Automotive Technology*, vol. 16, no. 3, pp. 417 – 426, 2015.

[24] V. K. Ambarisha and R. G. Parker, "Nonlinear dynamics of planetary gears using analytical and finite element models," *Journal of Sound and Vibration*, vol. 302, no. 3, pp. 577 – 595, 2007.

[25] H. Dong, K. Zhang, D. Wang, Y. Wu, and S. Bai, "Dynamic modeling of planetary gear train for vibration characteristic analysis," *Mechanisms and Machine Science*, vol. 31, pp. 187 – 195, 2015.

[26] A. Kahraman, "Natural modes of planetary gear trains," *Journal of Sound and Vibration*, vol. 173, no. 1, pp. 125 – 130, 1994.

[27] P.-Y. Wang and X.-L. Cai, "Vibrational analysis of planetary gear trains by finite element method," *Applied Mechanics and Materials*, vol. 284-287, pp. 1012 – 1017, 2013.

[28] N. Zhang, A. Crowther, D. Liu, and J. Jeyakumaran, "A finite element method for the dynamic analysis of automatic transmission gear shifting with a four-degree-of-freedom planetary gearset element," *Proceedings of the Institution of Mechanical Engineers, Part D: Journal*

of Automobile Engineering, vol. 217, no. 6, pp. 461 – 474, 2003.

[29] L. Zhang, Y. Wang, K. Wu, R. Sheng, and Q. Huang, "Dynamic modeling and vibration characteristics of a two-stage closed-form planetary gear train," *Mechanism and Machine Theory*, vol. 97, pp. 12 – 28, 2016.

[30] R. Parker, V. Agashe, and S. M. Vijayakar, "Dynamic response of a planetary gear system using a finite element/contact mechanics model," *Journal of Mechanical Design*, vol. 122, no. 3, pp. 304 – 310, 1999.

[31] A. Kahraman, "Free torsional vibration characteristics of compound planetary gear sets," *Mechanism and Machine Theory*, vol. 36, no. 8, pp. 953 – 971, 2001.

[32] A. Al-shyyab and A. Kahraman, "A non-linear dynamic model for planetary gear sets," *Proceedings of the Institution of Mechanical Engineers, Part K: Journal of Multi-body Dynamics*, vol. 221, no. 4, pp. 567 – 576, 2007.

[33] A. Al-shyyab and K. Alwidyan, "A nonlinear dynamic model for compound planetary gear sets," *3rd WSEAS International Conference on Applied And Theoretical Mechanics*, pp. 84 – 89, 2007.

[34] A. J. A. Al-shyyab, K. Al-Widyan and H. Tlilan, "Non-linear dynamic behaviour of compound planetary gear trains: model formulation and semi-analytical solution," *Proc. IMechE, Part K: J. of Multi-body Dynamics*, vol. 223, no. 3, pp. 199 – 210, 2009.

[35] M. Inalpolat and A. Kahraman, "Dynamic modelling of planetary gears of automatic transmissions," *Proceedings of the Institution of Mechanical Engineers, Part K: Journal of Multi-body Dynamics*, vol. 222, no. 3, pp. 229 – 242, 2008.

[36] T. Kailath, *Linear Systems*. Englewood Cliffs, N.J.: Prentice-Hall, 1980.

[37] K. Astrom and R. Murray, *Feedback Systems: An Introduction for Scientists and Engineers*. Princeton: Princeton University Press, 2008.

[38] N. Zhang, D. Liu, J. Jeyakumaran, and L. Villanueva, "Modelling of dynamic characteristics of an automatic transmission during shift changes," *Proc. IMechE, Part I: J. of Systems and Control Engineering*, vol. 216, no. 4, pp. 331 – 341, 2002.

Yuhanes D. Setiawan (M'15) received the B.Eng. degree in mechanical engineering from Diponegoro University, Semarang, Indonesia, and the M.Eng. degree in mechanical design engineering from Pukyong National University, Busan, South Korea. He is currently working toward the Ph.D. degree in mechanical engineering with McGill University, Montréal, Canada. His research focuses on improving electric vehicle performance by means of multi-speed transmissions.

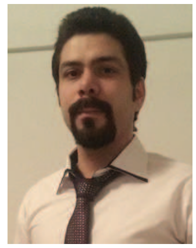

Mehdi Roozegar has received his B.Sc. and M.Sc. degrees in Mechanical Engineering from Shiraz University, Shiraz, Iran, in 2011 and University of Tehran, Tehran, Iran, in 2013, respectively. He is presently working towards his Ph.D. degree in the Centre for Intelligent Machines (CIM) at McGill University, Montréal, Canada. His research interests include modelling and control of multi-speed transmissions in electric vehicles (EVs), robotics, mechatronics, optimization and artificial intelligence.

Ting Zou is a Postdoctoral Fellow working with Prof. Angeles at the Centre for Intelligent Machines, McGill University. Dr. Zou obtained a B.Sc. in electrical engineering from Xi'an Jiaotong University in 2005, a M.Sc. in automatic control engineering from Xi'an Jiaotong University in 2008, and a Ph.D. degree in mechanical engineering from McGill University in 2013. Her research interests include design and optimization of robotic systems, automotive transmission system design and optimization.

Jorge Angeles (SM'90-F'06) received the Dipl.Eng. degree in electromechanical engineering and the M.Eng. degree in mechanical engineering from Universidad Nacional Autonoma de Mexico, Mexico City in 1969 and 1970, respectively, and the Ph.D. degree in applied mechanics from Stanford University, Stanford, CA, in 1973. In 1984, he joined the Department of Mechanical Engineering, McGill University, Montréal where, in 1985, he became a founding member of the Centre for Intelligent Machines and is currently James McGill Professor of Mechanical Engineering, and the Founder and Director of the Robotic Mechanical Systems Laboratory. Dr. Angeles is a Fellow of the RSC, The Academies of Arts, Humanities and Sciences of Canada. He is one of the 12 honorary members of IFToMM, the International Federation for the Promotion of Mechanism and Machine Science. He is a Fellow of the Canadian Society for Mechanical Engineers and the American Society of Mechanical Engineers. His professional registration as an Engineer includes Quebec, Mexico, and Germany.